Aeroelastic Characteristics of the Space Shuttle External Tank Cable Trays

L.E. Ericsson* and J. P. Reding†
Lockheed Missiles & Space Company, Sunnyvale, California

A study of the cable trays on the Space Shuttle external tank has shown that they are subject to high velocity crossflow, which causes flow separation. Preliminary aeroelastic analysis showed that the flow separation could endanger the structural integrity of the cable trays. A systematic experimental test program incorporating static and dynamic tests provided the information needed for a more definitive aeroelastic analysis, which is described in the present paper. The results of the analysis show that even when considering structural and geometric changes in the cable tray design since the initial analysis, the end result is the same, i.e., the structural integrity of the cable trays cannot be ensured. Consequently, various aerodynamic fixes were investigated to alleviate or possibly eliminate the adverse separated flow effects. The one selected consists of a 20-deg flow ramp that shields the cable trays from direct high-velocity crossflow.

Nomenclature

$\bar{A}$ = amplitude parameter, Eq. (7b)
c = two-dimensional chord length
c_0 = delta wing root chord
c_t = command module height (Fig. 8)
f = frequency
h = cross sectional height of cable tray (Fig. 3)
Δh = gap size (Fig. 3)
1 = sectional lift, coefficient $c_l = 1/(\rho V^2/2)c$
l = length of ground plane (Fig. 3)
M = Mach number
m_p = sectional pitching moment, coefficient $c_m = m_p/(\rho V^2/2)c^2$
r = corner radius
t = time
Δt = time lag
V = crossflow velocity
$\bar{V}$ = convection velocity
x = chordwise coordinate
α = angle of attack
Δ = increment and amplitude
ζ_0 = structural damping, fraction of critical
$\zeta_a + \zeta_s$ = aerodynamic damping, fraction of critical
θ = perturbation in pitch or torsion
λ = disturbance wave length
ν = kinematic viscosity of air
ξ = dimensionless x-coordinate, $\xi = x/c$
ξ_{sp} = effect of separation point movement, Eq. (12)
ξ_w = Karman-Sears wake lag parameter, Eq. (12)
ρ = air density
τ = dimensionless time, $\tau = Vt/c$
ϕ = phase angle, $\phi = \omega\Delta t$
$\omega, \bar{\omega}$ = oscillation frequency, $\bar{\omega} = \omega c/V$

Subscripts

a = attached flow
COMP = computed
L = linear range termination
MAX = maximum
s = separated flow
sp = separation point
tot = total
u = upstream
w = wake
0 = value at $\bar{\omega}^2 \ll 1$
∞ = freestream axial flow conditions

Superscript

$*$ = circulation-induced, c_l^* in Eq. (13)

Derivative Symbols

$c_{m\alpha}$ = $\partial c_m/\partial\alpha$
$\dot{\theta}$ = $\partial\theta/\partial t$: $\ddot{\theta} = \partial^2\theta/\partial t^2$
$c_{m\dot{\theta}}$ = $\partial c_m/\partial\left(\frac{c\dot{\theta}}{V}\right)$
$c_{\bar{m}\dot{\theta}}$ = integrated mean value

Presented as Paper 82-0633 at the AIAA/ASME/ASCE/AHS 23rd Structures, Structural Dynamics and Materials Conference, New Orleans, La., May 10-12, 1982; received May 24, 1982; revision received Oct. 17, 1983.

*Senior Consulting Engineer. Fellow AIAA.
†Staff Engineer. Associate Fellow AIAA.

Introduction

OF the various cable trays present on the main Space Shuttle booster, the hydrogen-oxygen (HO) tank (Fig. 1), the LO_2 cable tray was of special concern because of its low margin of safety. Examination of the LO_2 tank flowfield revealed that the interference from the nose of the adjacent solid rocket booster (SRB) subjects the LO_2 cable tray to large crossflow angles (up to 90 deg) at low supersonic vehicle velocities.[1] The rectangular cross section of the cable tray (Fig. 2) causes the crossflow over it to separate. The initial analysis[2] was made neglecting the presence of a pipe and the external tank (ground plane) surface (Fig. 2a). The later design with its added heat protection material brought the ground plane surface much closer (Fig. 2b), and its presence could no longer be neglected. Consequently, static and dynamic tests[1,3,4] were performed in a more or less two-dimensional flow arrangement (Fig. 3). The static test was performed only for a nominal sharp cornered cable tray configuration (Fig. 4a), but in the dynamic test a series of configurations (Fig. 4b) was investigated to define with the needed details the unsteady aerodynamics to be used in the final aeroelastic analysis.

Analytic Approach

Because of the problem of dynamic scaling, it was essential that the dynamic test data could be predicted using static experimental results. Figure 5 shows that the dynamic results of models 1 and 2 in Fig. 4b could be predicted rather well. Using the experimental dynamic results for model 2 (Fig. 4b) gave an aeroelastic stability boundary which was in remark-

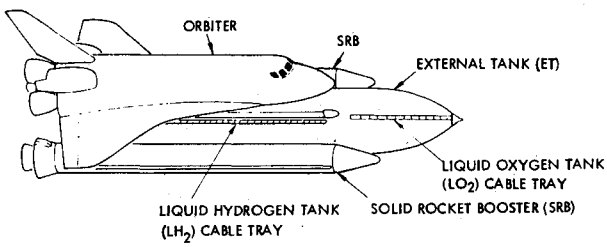

Fig. 1 Space Shuttle booster.

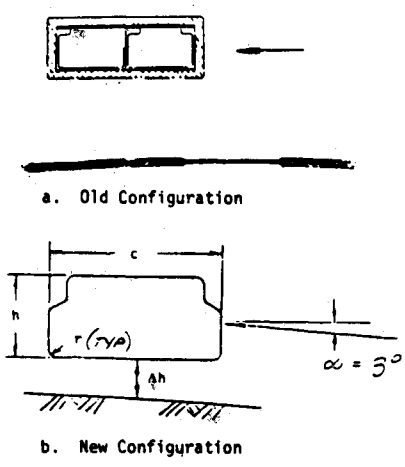

Fig. 2 Cable tray geometries.

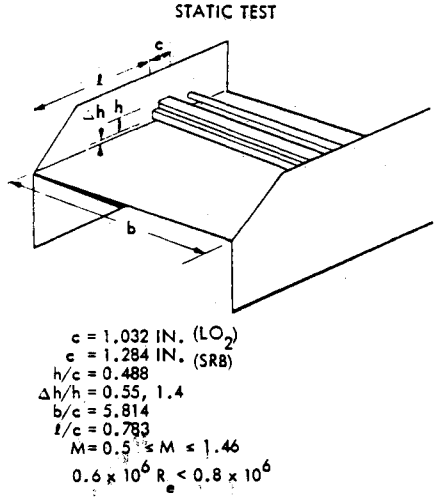

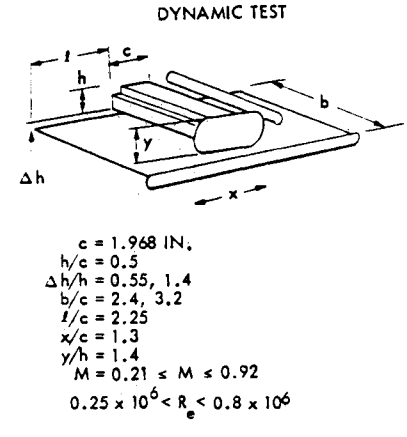

Fig. 3 Wind tunnel test arrangements.

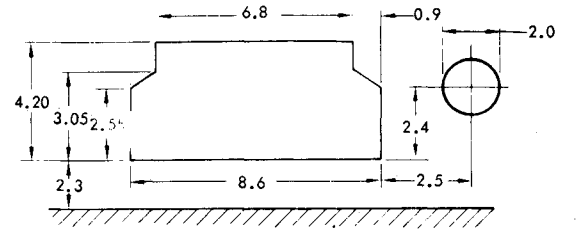

a. Static Test

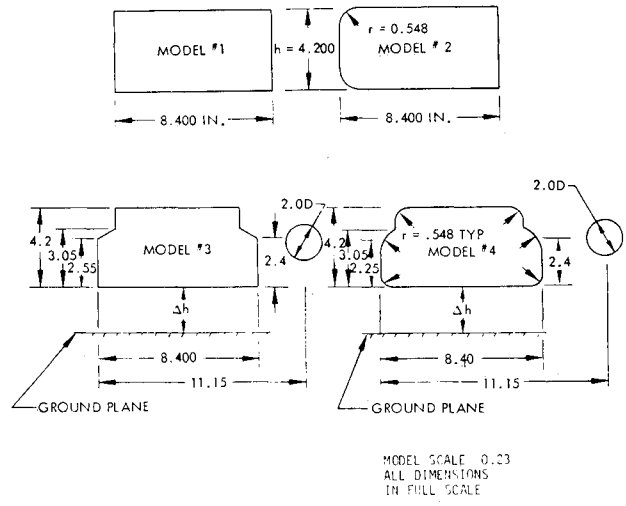

b. Dynamic Test

Fig. 4 Tested cable tray geometries.

ably good agreement with the preliminary (old) prediction of Ref. 1 (Fig. 6). However, the main concern was the analytic treatment of the nonlinear aerodynamics introduced by the severe ground plane interference experienced by the new cable tray geometry (Fig. 2b). Of particular importance was the determination of possible static hysteresis effects associated with the discontinuous change of cable tray characteristics at transonic crossflow velocities,[2] as they would generate nonlinear frequency effects.[5-7] The comparison between predicted[4] and measured[3] nonlinear dynamic characteristics showed no nonlinear frequency effect (Fig. 7). The static hysteresis effect is inversely proportional to the frequency for the measured dynamic stability parameter, i.e., the linear measure of energy dissipation per cycle.[5-7] Thus, the results in Fig. 7 prove that no static hysteresis was present, and that the developed analytic method for prediction of rigid body dynamics[4] was sufficiently accurate. This was a necessary prerequisite for the extension of the analysis to predict the aeroelastic characteristics of the Space Shuttle cable trays.

Aeroelastic Analysis

If the geometry had been the only change between the old and the new cable tray configurations (Figs. 2a and b, respectively) the new aeroelastic cable tray characteristics could have been computed utilizing the new sectional aerodynamics in the old aeroelastic analysis. (The analysis in Ref. 2 used linear structural representation, together with nonlinear aerodynamic characteristics, to determine the single degree of freedom response in bending or torsion. It was found that the critical response occurred in torsion, generating amplitudes that exceeded the structural capability of the LO_2 cable trays and supports, thus necessitating the use of protective flow ramps in the high crossflow region.) However, the new cable tray design

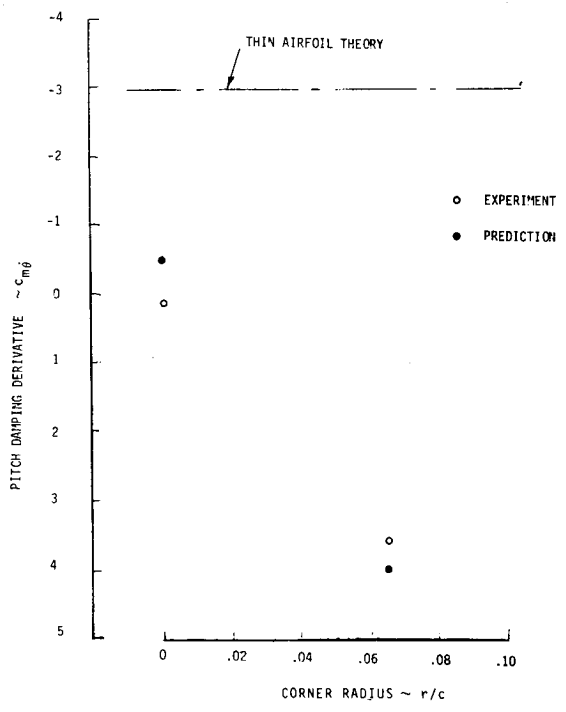

Fig. 5 Pitch damping of a rectangular cross section.

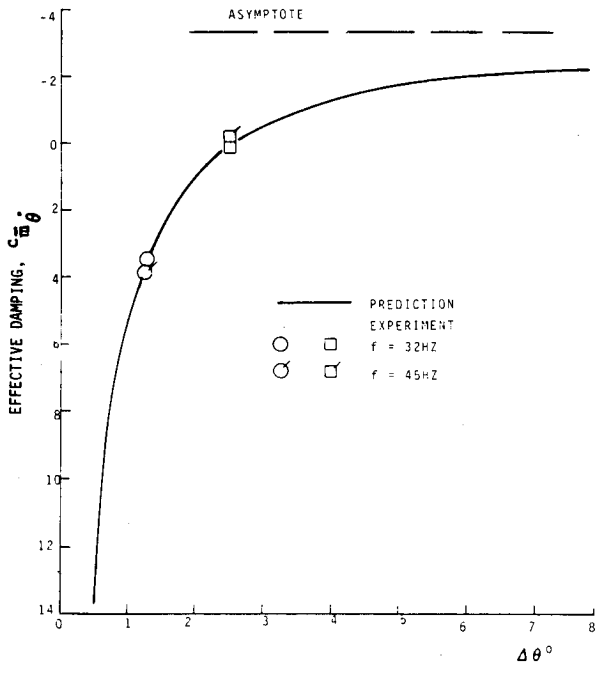

Fig. 7 Nonlinear damping characteristics of the LO_2 cable tray geometry at $M = 0.92$.

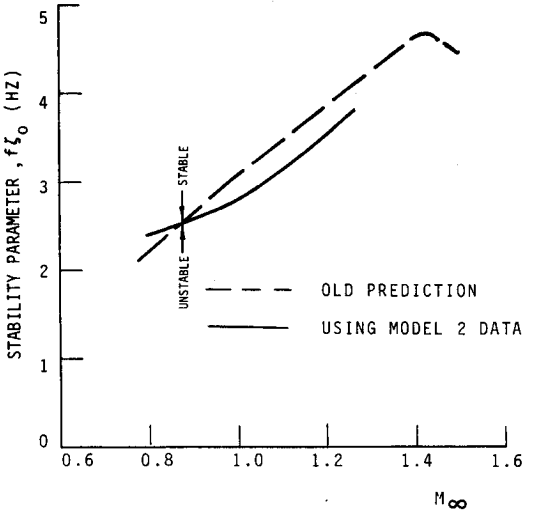

Fig. 6 Aeroelastic stability boundary.

had a load carrying lid, which increased the structural stiffness by an order of magnitude. As a result, the application of the unsteady cross sectional aerodynamics, which had been obtained at low reduced frequencies, to the elastic cable tray with its very much higher reduced frequencies, presented a dynamic scaling problem.

Dynamic Scaling

Complete dynamic simulation of, for example, the LO_2 cable tray in a subscale test is, for all practical purposes, impossible. What one is concerned with, rather, is the two-dimensional unsteady aerodynamics of the cable tray cross-section in presence of the external tank (ET) surface. These cross-sectional unsteady aerodynamic characteristics will be used to obtain the full scale aeroelastic characteristics of the cable tray, in the manner described in Ref. 2.

The use of dynamic derivatives builds upon the concept of linearity in a manner similar to what is the case for static derivatives. The static aerodynamic characteristics of an airfoil vary linearly with angle of attack up to a certain angle $\alpha = \alpha_L$, where beginning flow separation causes deviations and the characteristics become nonlinear. For $\alpha \le \alpha_L$ the static aerodynamics are described completely by the derivatives, e.g., $c_{l\alpha}$ and $c_{m\alpha}$. For perturbations in pitch, θ, around $\alpha = \alpha_0$ one has

$$\left.\begin{aligned} c_l &= c_l(\alpha_0) + c_{l\alpha}\theta \\ c_m &= c_m(\alpha_0) + c_{m\alpha}\theta \end{aligned}\right\} \tag{1}$$

provided that $|\alpha_0 + \theta| < \alpha_L$.

Extending the linear concept to the dynamic case of a pitching airfoil, one writes

$$\left.\begin{aligned} c_l &= c_l(\alpha_0) + c_{l\alpha}\theta + c_{l\dot{\theta}}\cdot\frac{c\dot{\theta}}{V} + c_{l\ddot{\theta}}\frac{c^2\ddot{\theta}}{V^2} \\ c_m &= c_m(\alpha_0) + c_{m\theta}\theta + c_{m\dot{\theta}}\frac{c\dot{\theta}}{V} + c_{m\ddot{\theta}}\frac{c^2\ddot{\theta}}{V^2} \end{aligned}\right\} \tag{2}$$

where θ, $c\dot{\theta}/V$ and $c^2\ddot{\theta}/V^2$ are measured in radians.

The aerodynamic inertia or acceleration terms, $c_{l\ddot{\theta}}(c^2\ddot{\theta}/V^2)$ and $c_{m\ddot{\theta}}(c^2\ddot{\theta}/V^2)$, are negligible compared to their structural counterparts. It is only the damping terms, $c_{l\dot{\theta}}(c\dot{\theta}/V)$ and $c_{m\dot{\theta}}(c\dot{\theta}/V)$, that are of concern. The contributions caused by nonzero pitch rate, $\dot{\theta} \neq 0$, can be written

$$\left.\begin{aligned} \Delta c_l(\dot{\theta}) &= c_l(\dot{\theta}) - c_l(0) \\ \Delta c_m(\dot{\theta}) &= c_m(\dot{\theta}) - c_m(0) \end{aligned}\right\} \tag{3}$$

These damping terms also have linear branches. In the case of a steadily increasing pitch rate, as in the pitch-up maneuver of an aircraft, one obtains a situation that is a direct extension of the static case. Thus, the linear characteristics prevail as long as

$$\left|\alpha_o + \theta + \frac{c\dot{\theta}}{V}\right| < \alpha_L \tag{4}$$

[This is a conservative value, as dynamic effects extend the linear branch beyond $\alpha = \alpha_L$ (Ref. 11).]

However, in the case of an airfoil that describes pitch oscillations around $\alpha = \alpha_o$, i.e., when

$$\left.\begin{aligned} \theta &= \Delta\theta \sin \omega t \\ \frac{c\dot{\theta}}{V} &= \frac{c\omega}{V}\Delta\theta \cos \omega t \end{aligned}\right\} \tag{5}$$

one finds that the magnitude of $c\dot{\theta}/V$ is

$$\left|\frac{c\dot{\theta}}{V}\right| = \bar{\omega}\Delta\theta \tag{6}$$

That is, $|c\dot{\theta}/V|$ is determined by two parameters, the pitch amplitude $\Delta\theta$ and the reduced frequency $\bar{\omega}$. How the two together affect airfoil characteristics, in attached and separated flow, has been described extensively in Refs. 8-11. These results will be used to delineate the applicability of the dynamic derivative concept.

For the case of attached flow, i.e., when Eq. (4) is satisfied, one is only concerned with the effect of the reduced frequency $\bar{\omega}$. More specifically, it must be determined to what extent the magnitude of $\bar{\omega}$ affects the applicability of $c_{l\dot{\theta}}$ and $c_{m\dot{\theta}}$. The only contributions to $c_{l\dot{\theta}}$ and $c_{m\dot{\theta}}$ that are sensitive to the magnitude of $\bar{\omega}$ come from the circulation terms. Reference 11 gives the following expression for the circulation lift (an analogous expression is obtained for the circulation effect on the pitching moment).

$$c_l^*(t) = c_l(\alpha_0) + c_{l\alpha}\bar{A}\Delta\theta \sin(\omega t - \phi) \tag{7a}$$

$$\bar{A} = \begin{cases} 1 & : \ \bar{\omega} < 0.16 \\ 0.475\left[1 - (10\bar{\omega})^{-1/2}\right] & : \ \bar{\omega} \geq 0.16 \end{cases} \tag{7b}$$

$$\phi = \begin{cases} 1.5\bar{\omega} & : \ \bar{\omega} < 0.16 \\ 14^\circ & : \ \bar{\omega} \geq 0.16 \end{cases} \tag{7c}$$

Expanding Eq. (7a), one obtains

$$c_l^*(t) = c_l(\alpha_0) + c_{l\alpha}\bar{A}\cos\phi\,\theta(t) - c_{l\alpha}\bar{A}\frac{\sin\phi}{\bar{\omega}}\frac{c\dot{\theta}(t)}{V} \tag{8}$$

which in turn gives

$$\partial c_l^* \Big/ \partial\left(\frac{c\dot{\theta}}{V}\right) = -c_{l\alpha}\bar{A}\frac{\sin\phi}{\bar{\omega}} \tag{9}$$

With the definitions in Eqs. (7b) and (7c), Eq. (9) gives

$$\frac{\partial c_l^*}{\partial\left(\frac{c\dot{\theta}}{V}\right)} = -1.5c_{l\alpha}\begin{cases} 1 & : \ \bar{\omega} < 0.16 \\ 0.475\left[\dfrac{0.16}{\bar{\omega}}\left(1 - \dfrac{1}{\sqrt{10\bar{\omega}}}\right)\right] & : \ \bar{\omega} \geq 0.16 \end{cases} \tag{10}$$

Equation (10) shows that the value of $c_{l\dot{\theta}}$ and $c_{m\dot{\theta}}$, measured at an arbitrary frequency below $\bar{\omega} = 0.16$, applies to the complete frequency range $\bar{\omega} < 0.16$. However, when applied to higher frequencies, $\bar{\omega} > 0.16$, measured attached flow derivatives would overestimate the contribution of the circulation lift.

It was shown in Ref. 10 that the phase lag limit, $\phi = 14$ deg, existing for attached flow, Eq. (7c), does not apply in the case of dynamic stall. The circulation lift can be expressed as follows

$$\left.\begin{aligned} c_{l_s}^*(t) &= c_{l\alpha_s}\alpha_i(t) \\ \alpha_i(t) &= \alpha_0 + \Delta\theta \sin(\omega t - \phi_{\text{tot}}) \\ \phi_{\text{tot}} &= \bar{\omega}\Delta\tau \end{aligned}\right\} \tag{11}$$

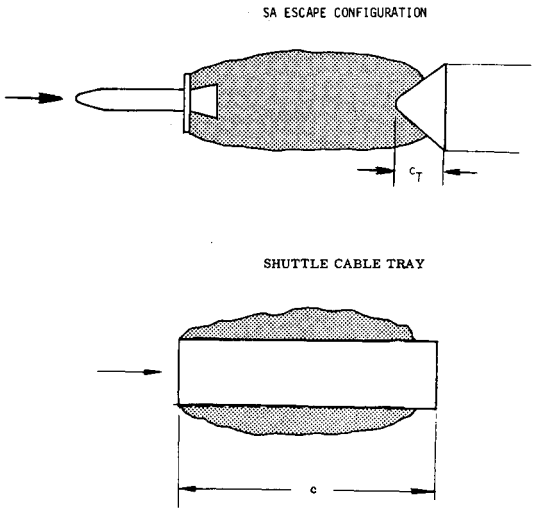

Fig. 8 Wavelength consideration for quasisteady methodology.

where $\Delta\tau$ is

$$\left.\begin{aligned} \Delta\tau &= \xi_w + \xi_{\text{sp}} \\ \xi_w &= 1.5 \\ \xi_{\text{sp}} &= \begin{cases} 0.75 & \text{Turbulent stall} \\ 3.0 & \text{Laminar stall} \end{cases} \end{aligned}\right\} \tag{12}$$

Again, with $\theta = \Delta\theta \sin \omega t$, expanding Eq. (11) gives

$$c_{l_{\dot{\theta}s}} = \partial c_{l_s}^*(t) \Big/ \partial\left(\frac{c\dot{\theta}}{V}\right) = -c_{l\alpha_s}\frac{\sin(\bar{\omega}\Delta\tau)}{\bar{\omega}} \tag{13}$$

For low reduced frequencies, as in the case of the dynamic tests,[3] Eq. (13) takes the following form

$$\left(c_{l_{\dot{\theta}s}}\right)_0 = -c_{l\alpha_s}\Delta\tau \tag{14}$$

Combining Eqs. (13) and (14) gives

$$c_{l_{\dot{\theta}s}} = \left(c_{l_{\dot{\theta}s}}\right)_o \frac{\sin(\bar{\omega}\Delta\tau)}{\bar{\omega}\Delta\tau} \tag{15}$$

Equation (15) implies that

$$\frac{c_{m_{\dot{\theta}s}}}{\left(c_{m_{\dot{\theta}s}}\right)_o} = \frac{c_{l_{\dot{\theta}s}}}{\left(c_{l_{\dot{\theta}s}}\right)_o} = \frac{\sin(\bar{\omega}\Delta\tau)}{\bar{\omega}\Delta\tau} \tag{16}$$

Equation (16) shows that applying the derivative measured at low frequency, $\bar{\omega}^2 \ll 1$, at $\bar{\omega}\Delta\tau = 1$ would overestimate the separated flow effect on the pitch damping by less than 20%.

In Eqs. (12) through (14) the aerodynamic derivative $c_{l\alpha_s}$ is obtained from static measurements. There is, of course, an upper limit in frequency for which this quasisteady approach will be applicable, on which the expressions in Eqs. (15) and (16) are based. In the axisymmetric separated flow case encountered for the Saturn-Apollo launch vehicle (Ref. 12 and Fig. 8) it can be assumed that when the separation distance between escape rocket and Apollo command module is large, so that no communication upstream from the command module affects the wake shape, the situation is analogous to that for a sinusoidal gust.[13] That is, the only consideration for the applicability of quasi-steady principles, i.e., use of static derivatives in a dynamic analysis, is that the wave length of the unsteady wake (or gust) is long compared to the extent of the responding body, e.g., the Apollo command module. A

minimum requirement for this is (see Fig. 8)

$$c_T < \lambda/4 \tag{17}$$

That is

$$\frac{\omega c_T}{V} < \frac{\pi}{2} \tag{18}$$

When the distance between wake generator, e.g., the escape rocket, and the submerged-body, e.g., the command module, is below a critical value, the wake reattachment conditions on the submerged body start to affect the wake formation at the upstream wake-generating body.[14] In this case one has to consider how the flow field effective time lag $\Delta\tau$ affects the wake in the unsteady case. That is, when does the phase lag ϕ_{tot} start to change the wake structure such that the static aerodynamic load distribution and associated lumped load derivative cannot be realized in the dynamic case? One minimum requirement for the application of static data is that the upstream communication effect, the modulation of the wake geometry, is of the same sense as in the static case. This would require that

$$\omega \Delta t_u < \pi \tag{19}$$

where

$$\Delta t_u = \frac{c_T}{\bar{V}_u} \tag{20}$$

with $\bar{V}_u$ being the upstream convection velocity. That is, Eq. (20) becomes

$$\bar{\omega} < \pi \bar{V}_u / V \tag{21}$$

where $\bar{\omega} = \omega c_\tau / V$.

Experimental results for wakes[15] indicates that the upstream convection will take place at a Mach number $M_u \geq 0.4$. Thus, for the subsonic and transonic flow conditions existing in the case of the cable trays one would have

$$\bar{V}_u / V > 0.4 \tag{22}$$

and Eq. (21) gives the very conservative value

$$\bar{\omega} < 0.4\pi \tag{23}$$

When considering the cable tray, the characteristic length is c rather than c_T (see Fig. 8), and the quasisteady gust criterion, Eq. (18), becomes

$$\bar{\omega} < 0.5\pi \tag{24}$$

which is not far from the criterion for quasisteadiness expressed in Eq. (23). If the upstream communication in the wake occurred through acoustic radiation rather than through convection, for the subsonic and transonic flow conditions of concern one would get

$$\bar{V}_u / V \geq 1 \tag{25}$$

and Eq. (23) would become

$$\bar{\omega} \leq \pi \tag{26}$$

Thus, one finds that the criterion for quasisteadiness used in past aeroelastic analyses of launch vehicles[5,16-18] still holds. That is, for the present aeroelastic analysis of the space shuttle cable trays the criterion for application of quasisteady principles, on which Eq. (16) is founded, is expressed by Eq. (24).

In addition to this consideration for $\bar{\omega}$, expressed by Eq. (24), one also has to take a closer look at ϕ_{tot}. In the case of attached flow $\phi_{tot} = \phi$ and does not exceed 14 deg, Eq. (7c). That this limit on ϕ_{tot} does not apply in the case of dynamic stall has been shown recently[10] (Fig. 9). The old predictions in Fig. 9a are far off the experimental results.[19] In Fig. 9b the 14 deg limit was removed, that is $\phi = 1.5\bar{\omega} = 61$ deg was used. It can be seen that this provided excellent agreement for the "upstroke" portion of the loop below stall, where $\phi_{tot} = \phi$. The deviation above stall between prediction and experiment can be explained when considering amplitude modulation effects, as is discussed in Ref. 10. The point to be made here is that the results in Fig. 9 prove that the phase lag can be as large as $\phi_{tot} = 61$ deg. The question is: How large can ϕ_{tot} be?

Experimental results for flow separation off the sharp leading edge of a delta wing[20] indicate that there might be an upper limit for ϕ_{tot} (Fig. 10). Figure 10a shows that the phase

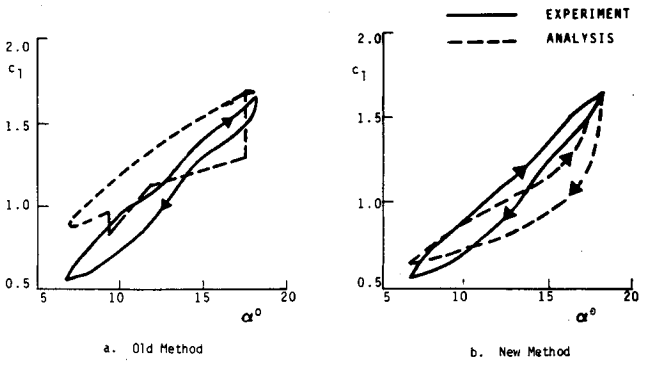

Fig. 9 Dynamic lift stall loops.

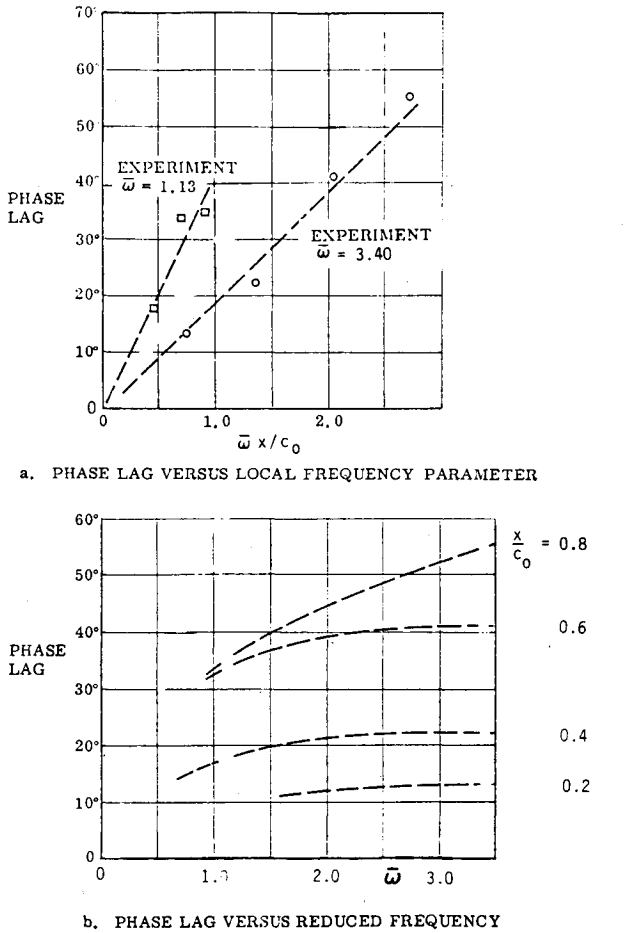

Fig. 10 Phase lag characteristics of a pitching sharp-edged delta wing (Ref. 20).

lag of the leading edge vortex location (height) above the delta wing is linearly dependent upon the distance from apex, but nonlinearly dependent upon the frequency. The nonlinear frequency effect is shown more clearly in Fig. 10b, illustrating how the experimental data trend is mathematically of a form similar to that given by Eq. (7c). It is apparent, however, that for separated flow the maximum phase angle is substantially higher than the 14 deg limit of Eq. (7c). The results in Fig. 10 give

$$\frac{\partial \phi_{\text{tot}}}{\partial\left(\frac{x}{c_o}\right)} = \begin{cases} 46° & : \ \bar{\omega} = 1.13 \\ 66° & : \ \bar{\omega} = 3.40 \end{cases} \tag{27}$$

The data trend in Fig. 10b indicates that the maximum phase lag that could be obtained on the delta wing, at $x/c_o = 1$, is $\phi_{\text{tot}} = 66$ deg.

The flow mechanisms leading to the phase lag saturation are very different in the attached flow case, Eq. (7c), and the delta wing leading edge separation just discussed. The results do suggest, however, that a phase lag limit is likely to exist also for the present case of interest, the separated flow past the cable tray cross section. Whatever this phase lag saturation limit is, one can state as a fact, at least for the flow processes that have been identified to affect the cable tray dynamics, that the aeroelastic analysis will give a conservative result if one assumes $\phi_{\text{tot}} \leq \pi/2$. That is, the low-frequency dynamic derivative, $(c_{m\theta_s})_o$, measured in the dynamic test[3] will be used as follows to provide the derivative, $c_{m\theta_s}$, needed in the aeroelastic analysis.

$$\frac{c_{m_{\theta s}}}{\left(c_{m_{\theta s}}\right)_o} = \begin{cases} \dfrac{\sin(\bar{\omega}\Delta\tau)}{\bar{\omega}\Delta\tau} & : \ \bar{\omega}\Delta\tau < \dfrac{\pi}{2} \\ (\bar{\omega}\Delta\tau)^{-1} & : \ \bar{\omega}\Delta\tau \geq \dfrac{\pi}{2} \end{cases} \tag{28}$$

Aeroelastic Characteristics of the Final Cable Tray Design

Because of the very high frequency computed for the revised structural characteristics, Eq. (28) reduces to the following for oscillations of the current cable trays.

$$c_{m\theta_s}/\left(c_{m\theta_s}\right)_0 = 1/(\bar{\omega}\Delta\tau) \tag{29}$$

where subscript zero designates the damping derivative measured in the dynamic test.[3] For continuous aerodynamics, $M < M_a$, $(c_{m\theta_s})_o$ for the two trays is obtained from Ref. 3. Figure 11 demonstrates that the LO_2 cable tray is aeroelastically stable for $M < M_a$, even if the structural damping reaches the minimum level of 0.1% (Ref. 21).

For the discontinuous aerodynamics at $M = 0.7$ and $M = 0.92$ (Ref. 1), the time lag is[22,23]

$$\left.\begin{aligned} M = 0.7 \quad &: \quad \Delta\tau = 4.0 \\ M = 0.92 \quad &: \quad \Delta\tau = 2.8 \end{aligned}\right\} \tag{30}$$

Using the measured damping derivatives[3] and the scaling relationships given by Eqs. (29) and (30) in the aeroelastic analysis described in Ref. 2 gives the aeroelastic stability

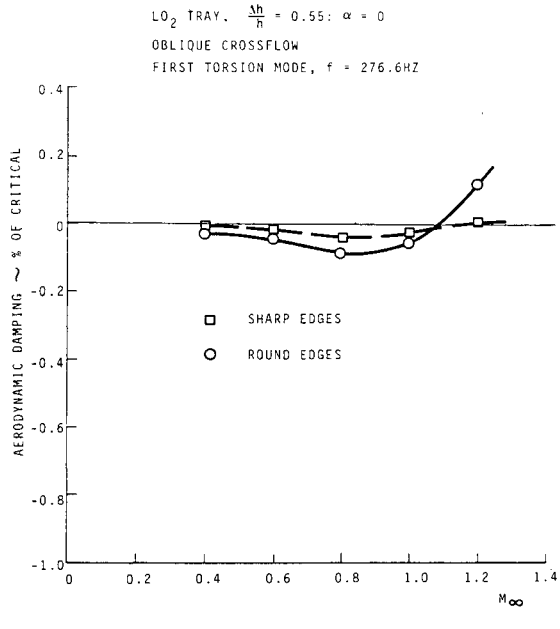

Fig. 11 Linear aeroelastic torsional characteristics of the LO_2 cable tray.

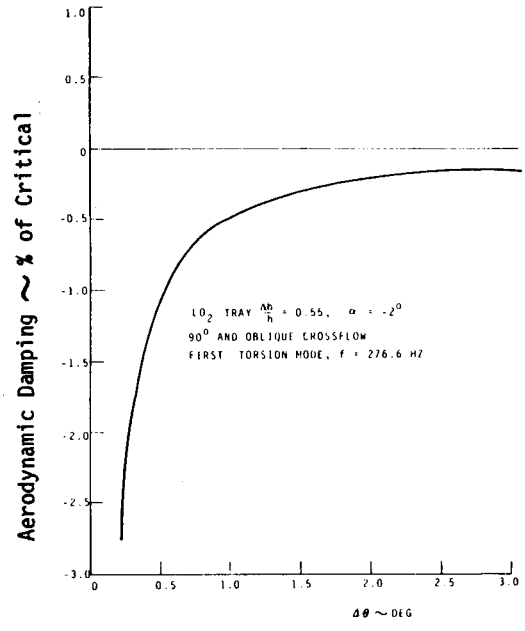

a. M = 0.7

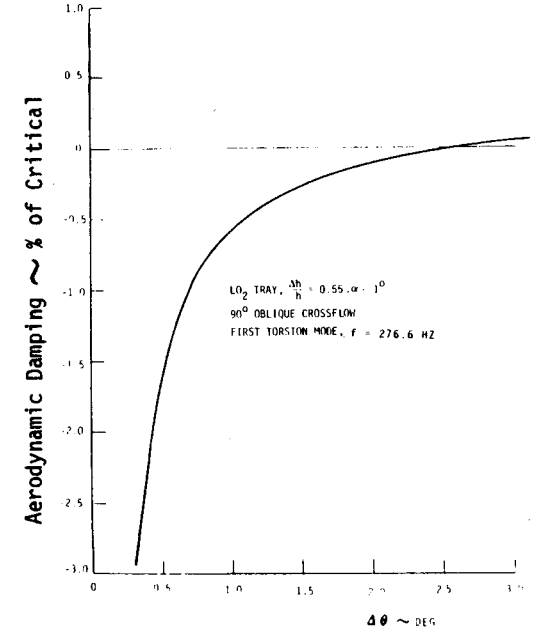

b. M = 0.92

Fig. 12 Nonlinear aeroelastic torsional characteristics of the LO_2 cable tray.

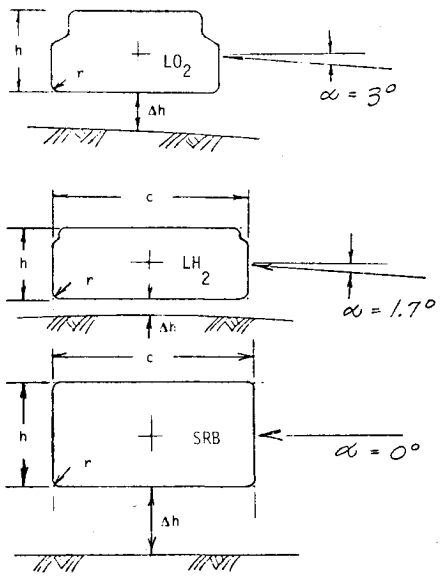

Fig. 13 Current cable tray geometries.

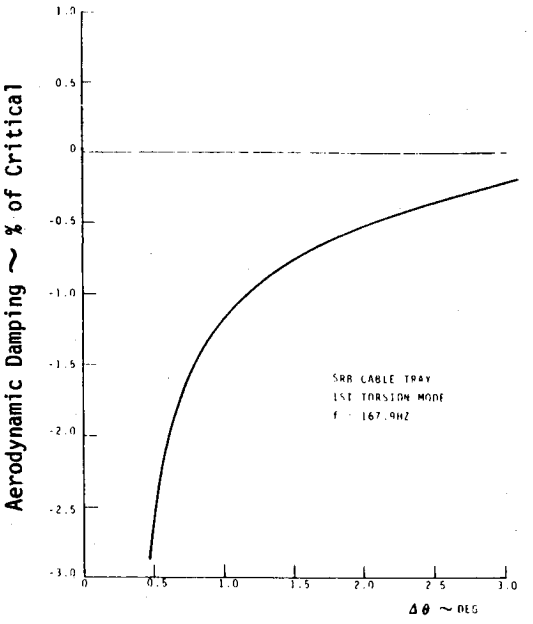

a. M = 0.7

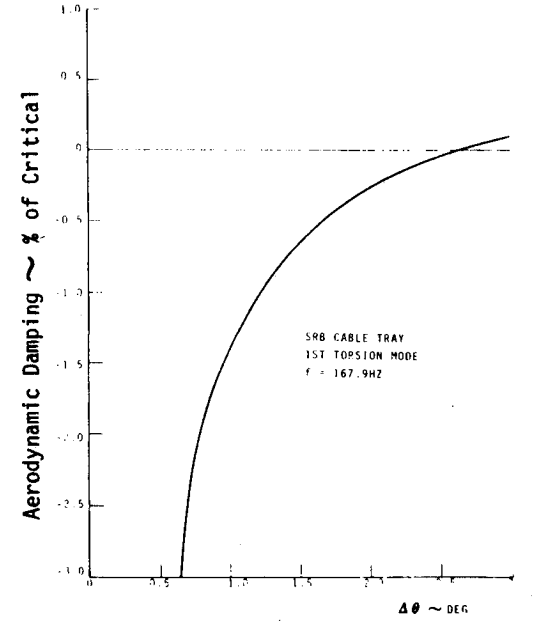

b. M = 0.92

Fig. 14 Nonlinear aeroelastic torsional characteristics of the SRB cable tray.

characteristics shown in Fig. 12. The results indicate that for the guaranteed value of $\zeta_o = 0.1\%$ (Ref. 21) the limit cycle amplitudes are $\Delta\theta_{LIM} > 3$ deg and $\Delta\theta_{LIM} = 2.1$ deg for $M = 0.7$ and $M = 0.92$, respectively. If the structural damping is one order of magnitude larger, $\zeta_o = 1\%$, the limit cycle amplitude decrease to 0.55 and 0.70 degs, respectively. $\zeta_o = 0.01$ is the highest structural damping value that can be expected according to limited shake tests.

Without any available experimental data that truly represents the LH_2 or SRB cable trays, one has to decide to what extent the experimental results for the LO_2 tray[3] can be used to determine the aeroelastic stability characteristics of the other cable trays. In regard to the LH_2 cable tray, three-dimensional flow effects add to the difficulty of using two-dimensional aerodynamic characteristics obtained with the wrong cross section (Fig. 13), and no meaningful aeroelastic prediction can be made. In regard to the SRB tray, however, the LO_2 tray aerodynamics should apply. If one neglects the effect of the forward indentation on the topside flow, which may be somewhat unconservative, the LO_2 cable tray aerodynamics can be applied directly to the SRB cable tray (see Fig. 13). For the first torsion mode the results in Fig. 14 are obtained, showing the rather substantial limit cycle amplitude $\Delta\theta_{LIM} \approx 1.2$ deg for 1% structural damping, both at $M = M_\infty = 0.7$ and $M = M_\infty = 0.92$.

Even for the maximum value of structural damping, $\zeta_o = 0.01$, the limit cycle amplitudes computed for the LO_2 and SRB cable trays exceed the structural capability. Consequently, the final analysis gives the same end result as the initial one,[1] i.e., an aerodynamic fix, such as the investigated 20 deg flow ramp,[1,3] is needed to assure the structural integrity of the LO_2 and SRB cable trays. Now as before,[2] the results for the LH_2 cable tray are inclusive, and the flow ramp has to be applied in the inflow regions of the LH_2 cable tray until more definitive results are obtained from currently planned analytic and experimental efforts. Until then, the Space Shuttle continues to carry protective crossflow ramps.

Conclusions

An analysis of the aeroelastic stability of the Space Shuttle cable trays has produced results that can be summarized as follows:

1) Using the c_m-discontinuities defined by static test data, the measured nonlinear pitch damping characteristics of the LO_2 cable tray cross section can be predicted by the developed analytic means.

2) A careful look at the dynamic scaling shows how to apply the low-frequency, cross-sectional dynamic test data to obtain a conservative estimate of the aeroelastic stability of high frequency torsion modes of the cable tray.

3) Using conservative assumptions, the dynamic test data for the LO_2 cable tray section have been used to determine the aeroelastic stability of the SRB cable tray.

4) The analysis confirms the need for the protective crossflow ramps now installed on the Space Shuttle launch vehicle to assure the structural integrity of the cable trays.

Acknowledgments

The paper is based upon results obtained in work done under contract to Martin-Marietta Corporation, Michoud Operations, New Orleans, La., with Mr. D.B. Schwartz as the Contract Coordinator.

The authors want to acknowledge that significant contributions to the presented analysis were made by the participants in the ET Protuberance Airloads Committee Meetings, in particular by W. Dahm and G.A. Wilhold, NASA MSFC.

References

[1]Reding, J.P. and Ericsson, L.E., "Analysis of Static and Dynamic Wind Tunnel Tests of the Space Shuttle Cable Trays," *Journal of Spacecraft and Rockets*, Vol. 19, Sept.-Oct. 1982, pp. 412-418.

[2]Ericsson, L.E. and Reding, J.P., "Aeroelastic Stability of Space Shuttle Protuberances," *Journal of Spacecraft and Rockets*, Vol. 19, July-Aug. 1982, pp. 307-313.

[3]Orlik-Rückemann, K.J. and LaBerge, J.G., "Dynamic Wind Tunnel Tests of The Simulated Shuttle External Tank Cable Trays," *Journal of Spacecraft and Rockets*, Vol. 20, Jan.-Feb. 1983, pp. 5-10.

[4]Ericsson, L.E. and Reding, J.P., "Separated Flow Dynamics of the Space Shuttle Cable Trays," AIAA Paper No. 81-1880, Aug. 1981.

[5]Ericsson, L.E. and Reding, J.P., "Dynamics of Separated Flow Over Blunt Bodies," NASA CR-76912, Dec. 1965.

[6]Ericsson, L.E., "Separated Flow Effects on the Static and Dynamic Stability of Blunt Nosed Cylinder Flare Bodies," NASA CR-76919, Dec. 1965.

[7]Ericsson, L.E., "Unsteady Aerodynamics of Separating and Reattaching Flow on Bodies of Revolution," *Recent Research on Unsteady Boundary Layers*, Vol. 1, International Union of Theoretical and Applied Mechanics Symposium, Laval University, Quebec, Canada, May 24-28, 1971, pp. 481-512.

[8]Ericsson, L.E. and Reding, J.P., "Dynamic Stall Analysis in Light of Recent Numerical and Experimental Results," *Journal of Aircraft*, Vol. 13, April 1976, pp. 248-255.

[9]Ericsson, L.E. and Reding, J.P., "Quasi-Steady and Transient Dynamic Stall Characteristics," Paper 24, AGARD CP-204, Feb. 1977.

[10]Ericsson, L.E. and Reding, "Dynamic Stall at High Frequency and Large Amplitudes," *Journal of Aircraft*, Vol. 17, March 1980, pp. 136-142.

[11]Ericsson, L.E. and Reding, J.P., "Unsteady Airfoil Stall, Review and Extension," *Journal of Aircraft*, Vol. 8, Aug. 1971, pp. 609-616.

[12]Ericsson, L.E. and Reding, J.P., "Analysis of Flow Separation Effects on the Dynamics of a Large Space Booster," *Journal of Spacecraft and Rockets*, Vol. 2, July-Aug. 1965, pp. 481-490.

[13]Ericsson, L.E., Reding, J.P., and Guenther, R.A., "Elastic Launch Vehicle Response to Sinusoidal Gusts," *Journal of Spacecraft and Rockets*, Vol. 10, April 1973, pp. 244-258.

[14]Ericsson, L.E., Reding, J.P., and Guenther, R.A., "Analytic Difficulties in Predicting Dynamic Effects of Separated Flow," *Journal of Spacecraft and Rockets*, Vol. 8, Aug. 1971, pp. 872-878.

[15]Ericsson, L.E. and Reding, J.P., "Transonic Sting Interference," *Journal of Spacecraft and Rockets*, Vol. 17, March-April 1980, pp. 140-144.

[16]Ericsson, L.E., "Aeroelastic Instability Caused by Slender Payloads," *Journal of Spacecraft and Rockets*, Vol. 4, Jan. 1967, pp. 65-73.

[17]Reding, J.P. and Ericsson, L.E., "Aeroelastic Stability of the 747/Orbiter," *Journal of Aircraft*, Vol. 14, Oct. 1977, pp. 988-993.

[18]Reding, J.P. and Ericsson, L.E., "Effects of Flow Separation on Shuttle Longitudinal Dynamics and Aeroelastic Stability," *Journal of Spacecraft and Rockets*, Vol. 14, Dec. 1977, pp. 711-718.

[19]Liiva, J., Davenport, F.J., Gray, L., and Walton, I.C., "Two-Dimensional Tests of Airfoils Oscillating Near Stall," USA AVLABS TR 68-13, April 1968.

[20]Maltby, R.L., Engler, P.B., and Keating, R.F.A., with addendum by Moss, G.F., "Some Exploratory Measurements of Leading-Edge Vortex Positions on a Delta Wing Oscillating in Heave," Aeronautical Research Council of Great Britain, R & M 3176, July 1963.

[21]Crema, L.B., Castellani, A., and Nappi, A., "Damping Effects in Joints and Experimental Tests on Riveted Specimens," Paper 12, AGARD-CP-277, Oct. 1979.

[22]Ericsson, L.E. and Reding, J.P., "Shock-Induced Dynamic Stall," *Journal of Aircraft*, Vol. 21, May 1984, pp. 316-321.

[23]Ericsson, L.E. and Reding, J.P., "Subsonic Dynamic Stall in Pitching and Plunging Oscillations Including Large Ground Interference Effects," AIAA Paper 83-0889-CP, May 1983.